The Journal of Chemical Physics ARTICLE scitation.org/journal/jcp

Self-consistent construction of grand potential functional with hierarchical integral equations and its application to solvation thermodynamics

Cite as: J. Chem. Phys. 156, 054116 (2022); doi: 10.1063/5.0079806
Submitted: 24 November 2021 • Accepted: 18 January 2022 •
Published Online: 7 February 2022

Tomoaki Yagi[1,a] and Hirofumi Sato[1,2,3,b]

AFFILIATIONS

[1] Department of Molecular Engineering, Graduate School of Engineering, Kyoto University, Kyoto 615-8510, Japan
[2] Elements Strategy Initiative for Catalysts and Batteries (ESICB), Kyoto University, Kyoto 615-8520, Japan
[3] Fukui Institute for Fundamental Chemistry, Kyoto University, Kyoto 606-8103, Japan

[a] **Author to whom correspondence should be addressed:** yagi@riron.moleng.kyoto-u.ac.jp
[b] **Electronic mail:** hirofumi@moleng.kyoto-u.ac.jp

ABSTRACT

The construction of the density functional for grand potential is fundamental in understanding a broad range of interesting physical phenomena, such as phase equilibrium, interfacial thermodynamics, and solvation. However, the knowledge of a general functional accurately describing the many-body correlation of molecules is far from complete. Here, we propose a self-consistent construction of the grand potential functional based on the weighted density approximation (WDA) utilizing hierarchical integral equations. Different from our previous study [T. Yagi and H. Sato, J. Chem. Phys. **154**, 124113, (2021)], we apply the WDA to the excess Helmholtz free energy functional rather than the bridge functional. To assess the performance of the present functional, we apply it to the solvation thermodynamics of Lennard-Jones fluids. Compared to the modified Benedict–Webb–Rubin equation of state, the present functional qualitatively predicts the liquid–vapor equilibrium. The solvation free energy obtained from the present functional provides a much better agreement with the Monte Carlo simulation result than the hypernetted chain functionals. It constitutes a general starting point for a systematic improvement in the accuracy of the grand potential functional.

I. INTRODUCTION

Grand potential is a fundamental thermodynamic quantity for open systems. It is the heart of a broad range of interesting physical phenomena, such as phase equilibrium, interfacial thermodynamics, and solvation.

The density functional theory (DFT) provides the rigorous foundation that proves the existence of a density functional of the grand potential and shows that it is minimal for the equilibrium density profiles.[1,2] For applications, the main problem is to construct a functional of the excess free energy, which contains all the information about the inter-particle correlation, for the system of interest.

One option for constructing the grand potential functional is the density expansion of the excess free energy functional. The Taylor expansion of the excess free energy around a uniform bulk density gives the grand potential functional as an infinite series of multi-body integrals. In the DFT language, the hypernetted-chain (HNC) approximation can be understood as the second-order truncation of the density expansion.[3] The weakness of the HNC approximation has been reported by various authors.[4–11] Owing to the quadratic expansion, the HNC is unable to describe a grand potential energy density with two minima necessary to account for the liquid–vapor equilibrium. Consequently, it largely overestimates the energy cost for the creation of a cavity (a gas bubble). Although this has to be corrected by including the excess functional for higher-order correlations, the so-called bridge functional,[3] it is practically infeasible to perform the numerical calculation of the n-body integral ($n \geq 3$) without any approximation.

Ideally, one would like to treat the higher-order correlation as an integral over an effective one-body function instead of a multi-body integral. The weighted-density approximation (WDA)

provides the one-body integral that would be a good approximation for the excess free energy functional.[12–24] In the WDA approach, the excess free energy is approximated as the one-body integral of the excess free energy density at a smoothed average density, determined from a suitably weighted average of the actual nonuniform density distribution. Different versions of the WDA mainly differ in the procedure for the calculation of the smoothed density calculated by (1) local averaging,[12–19] (2) global averaging,[20–22] or (3) a hybrid of both local and global averaging.[23,24] The fundamental measure theory (FMT),[25–33] which gives the most successful and most accurate free energy functional for hard-sphere mixtures, is also categorized into the WDA approach. However, because the WDA requires the analytical expression of the free energy as a function of density, the application is limited to the system whose equation of state is already known.

The combination of the density expansion method and the WDA has also been developed. One attempt is the hard-sphere reference functional method (HSRF) that employs the hard-sphere functional obtained from the WDA as a reference functional for the density expansion.[5,6,9] In this method, the diameter of the hard-sphere is empirically adjusted to reproduce the property of the system of interest. Recently, Borgis *et al.* proposed the ansatz for the bridge part of the free energy density, which is parameterized with empirical thermodynamic properties of the bulk solvent.[10,11] The WDA for the bridge functional with this free energy density gives accurate hydration energies for organic molecules compared with molecular simulation and experiment.

Summarizing the aim of this work, the question we set out to answer is how to construct the quantitatively accurate grand potential functional only from the pair potential. The reason is that empirical density functionals lack the versatility to support applications on a wide variety of systems. Very recently, we presented a novel scheme to self-consistently construct the bridge functional based on the WDA.[34] The bridge functional gives the improvements on the HNC approximation. In this study, we apply the WDA to the excess Helmholtz free energy functional rather than the bridge functional to refine the definition of the weight function. The resulting functional is self-consistently obtained from hierarchical integral equations. We test the functional with the application to the solvation thermodynamics of Lennard-Jones fluids.

The outline of this paper is as follows: In Sec. II, through the density expansion of the excess Helmholtz free energy functional, we derive the grand potential functional in terms of the direct correlation functions (DCFs) that are obtained from self-consistent hierarchical integral equations. In Sec. III, as an illustration, the present functional is applied to the liquid–vapor equilibrium and the solvation thermodynamics of Lennard-Jones fluids. Conclusions are given in Sec. IV.

II. THEORY

A. Grand potential functional and weighted density approximation

We consider a grand canonical ensemble of one component system under an external field whose grand potential is given as a density functional,

$$\Omega[n;\mu-v]=\mathscr{F}[n]-\int \mathrm{d}\boldsymbol{r}n(\boldsymbol{r})\{\mu-v(\boldsymbol{r})\}, \tag{1}$$

where n is the number density distribution, μ is the chemical potential, and v is the external field. $\mathscr{F}$ is the Helmholtz free energy, which can be decomposed into the ideal part and the excess part,

$$\mathscr{F}[n]=\mathscr{F}^{\mathrm{id}}[n]+\mathscr{F}^{\mathrm{ex}}[n], \tag{2}$$

$$\mathscr{F}^{\mathrm{id}}[n]=k_BT\int \mathrm{d}\boldsymbol{r}n(\boldsymbol{r})\left[\ln\left(n(\boldsymbol{r})\Lambda^3\right)+1\right], \tag{3}$$

where T is the temperature, k_B is the Boltzmann constant, and Λ is the thermal de Broglie wavelength. While the ideal part is given as the analytical expression, the general functional form of the excess part is unknown.

We consider the density functional of the grand potential relative to the equilibrium uniform system, $n=n_0$, as follows:

$$\Delta\Omega[n;\mu(n_0)-v]\equiv\Omega[n;\mu(n_0)-v]-\Omega[n_0;\mu(n_0)], \tag{4}$$

$$=k_BT\left[\int \mathrm{d}\boldsymbol{r}n(\boldsymbol{r})\ln\left(\frac{n(\boldsymbol{r})}{n_0}\right)-\int \mathrm{d}\boldsymbol{r}\Delta n(\boldsymbol{r})\right]+\Delta\mathscr{F}^{\mathrm{ex}}[n,n_0]-\mu^{\mathrm{ex}}(n_0)\int \mathrm{d}\boldsymbol{r}\Delta n(\boldsymbol{r})+\int \mathrm{d}\boldsymbol{r}n(\boldsymbol{r})v(\boldsymbol{r}), \tag{5}$$

where $\Delta n(\boldsymbol{r})=n(\boldsymbol{r})-n_0$ and $\Delta\mathscr{F}^{\mathrm{ex}}[n,n_0]=\mathscr{F}^{\mathrm{ex}}[n]-\mathscr{F}^{\mathrm{ex}}[n_0]$. We perform the Taylor expansion of the excess Helmholtz free energy around the uniform density n_0 as follows:

$$\Delta\mathscr{F}^{\mathrm{ex}}[n,n_0]=\int \mathrm{d}\boldsymbol{r}_1\phi^{\mathrm{ex}}[n,n_0](\boldsymbol{r}_1)\Delta n(\boldsymbol{r}_1), \tag{6}$$

$$\phi^{\mathrm{ex}}[n,n_0](\boldsymbol{r}_1)\equiv\mu^{\mathrm{ex}}(n_0)-\sum_{m=2}^{\infty}\frac{1}{m!}\int \mathrm{d}\boldsymbol{r}_2\ldots\int \mathrm{d}\boldsymbol{r}_m c^{(m)}(\boldsymbol{r}_{21},\ldots,\boldsymbol{r}_{m1};n_0)\times\Delta n(\boldsymbol{r}_2)\ldots\Delta n(\boldsymbol{r}_m), \tag{7}$$

where $c^{(m)}$ represents the mth-order direct correlation function (DCF),

$$c^{(m)}(\boldsymbol{r}_{21},\ldots,\boldsymbol{r}_{m1};n_0)\equiv-\frac{1}{k_BT}\frac{\delta m\mathscr{F}^{\mathrm{ex}}[n]}{\delta n(\boldsymbol{r}_1)\ldots\delta n(\boldsymbol{r}_m)}\bigg|_{n=n_0}. \tag{8}$$

ϕ^{ex} is the local excess Helmholtz free energy per excess particle number. For uniform density, $n(\boldsymbol{r})=n$, ϕ^{ex} is given as a function of density,

$$\phi^{\mathrm{ex}}[n,n_0]=\phi_0^{\mathrm{ex}}(n,n_0)=\mu^{\mathrm{ex}}(n_0)-\sum_{m=2}^{\infty}\frac{k_BT}{m!}C^{(m)}(n_0)\Delta n^{m-1}, \tag{9}$$

where $C^{(m)}(n_0)$ is the Fourier transform of DCF at zero wave vector,

$$C^{(m)}(n_0)\equiv\hat{c}^{(m)}(\boldsymbol{0},\ldots,\boldsymbol{0};n_0), \tag{10}$$

$$\hat{c}^{(m)}(\boldsymbol{k}_2,\ldots,\boldsymbol{k}_m;n_0)=\int \mathrm{d}\boldsymbol{r}_2\ldots\int \mathrm{d}\boldsymbol{r}_m e^{-i(\boldsymbol{r}_2\cdot\boldsymbol{k}_2+\cdots+\boldsymbol{r}_m\cdot\boldsymbol{k}_m)}\times c^{(m)}(\boldsymbol{r}_{21},\ldots,\boldsymbol{r}_{m1};n_0). \tag{11}$$

The hat indicates the Fourier transform in the following.

Owing to the difficulty of numerical calculation of the n-body integral ($n \geq 3$), the density expansion is practically unusable. Here, we introduce the effective density to obtain the excess Helmholtz free energy functional as a tractable form. The effective density, n^{eff}, is defined to satisfy the following equation:

$$\phi^{\mathrm{ex}}[n, n_0](\boldsymbol{r}) \equiv \phi_0^{\mathrm{ex}}\left(n^{\mathrm{eff}}[n](\boldsymbol{r}), n_0\right). \tag{12}$$

We perform the linear approximation around the uniform density, n_0, for the effective density as

$$n^{\mathrm{eff}}[n](\boldsymbol{r}) \approx n_0 + \int \mathrm{d}\underline{\boldsymbol{r}}_1 w(|\boldsymbol{r} - \underline{\boldsymbol{r}}_1|; n_0)\Delta n(\underline{\boldsymbol{r}}_1), \tag{13}$$

$$w(|\boldsymbol{r}_1 - \boldsymbol{r}_2|; n_0) \equiv \left.\frac{\delta n^{\mathrm{eff}}[n](\boldsymbol{r}_1)}{\delta n(\boldsymbol{r}_2)}\right|_{n=n_0}. \tag{14}$$

Inserting Eqs. (6), (12), and (14) into the definition of the second-order DCF [Eq. (8)], we obtain the weight function w as the normalized second-order DCF,

$$w(|\boldsymbol{r}_1 - \boldsymbol{r}_2|; n_0) = \frac{c^{(2)}(|\boldsymbol{r}_1 - \boldsymbol{r}_2|; n_0)}{C^{(2)}(n_0)}. \tag{15}$$

In general, although the structure factor $S^{-1}(r) = \delta(r)/n_0 - c^{(2)}(r)$ is positive definite, the DCF $-c^{(2)}(r)$ is not positive definite. Thus, the weight function w is also not positive definite. However, since w is normalized as $\hat{w}(0) = 1$, the weight function holds the conservation of mass for the effective density. Inserting Eqs. (6), (9), and (12) into Eq. (5), we approximately obtain the grand potential as

$$\begin{aligned}
&\Delta\Omega[n; \mu(n_0) - v] \\
&\quad = k_B T\left[\int \mathrm{d}\boldsymbol{r} n(\boldsymbol{r}) \ln\left(\frac{n(\boldsymbol{r})}{n_0}\right) - \int \mathrm{d}\boldsymbol{r}\Delta n(\boldsymbol{r})\right] \\
&\qquad + \int \mathrm{d}\boldsymbol{r} n(\boldsymbol{r}) v(\boldsymbol{r}) \\
&\qquad - \frac{k_B T}{2}\int \mathrm{d}\boldsymbol{r}_1 \int \mathrm{d}\boldsymbol{r}_2 c^{(2)}(|\boldsymbol{r}_1 - \boldsymbol{r}_2|)\Delta n(\boldsymbol{r}_1)\Delta n(\boldsymbol{r}_2) \\
&\qquad - \sum_{m=3}^{\infty} \frac{k_B T}{m!} C^{(m)}(n_0) \int \mathrm{d}\boldsymbol{r}_1 \left(\Delta n^{\mathrm{eff}}(\boldsymbol{r}_1)\right)^{m-1} \Delta n(\boldsymbol{r}_1).
\end{aligned} \tag{16}$$

The n-body integrals ($n \geq 3$) in Eq. (7) are replaced by one-body integrals. The truncation of the last line equals the HNC approximation. To obtain the grand potential functional, we need to calculate the second-order DCF, $c^{(2)}(r; n_0)$, and the Fourier transform of DCF at zero wave vector, $C^{(i)}(n_0)$ ($i = 3, \ldots, m$).

B. Self-consistent hierarchical integral equations for DCFs

From the variational principle for the grand potential, the equilibrium density distribution under the external potential $v(\boldsymbol{r})$ is given by the Boltzmann factor of the effective potential v^{eff},

$$n_{\mathrm{eq}}[\mu(n_0) - v](\boldsymbol{r}) = n_0 \exp\left(-\beta v^{\mathrm{eff}}[n_{\mathrm{eq}}](\boldsymbol{r})\right), \tag{17}$$

$$v^{\mathrm{eff}}[n](\boldsymbol{r}) = v(\boldsymbol{r}) + \Delta\mu^{\mathrm{ex}}[n](\boldsymbol{r}), \tag{18}$$

where $\beta = 1/k_B T$ is the inverse temperature. We define the local excess chemical potential relative to bulk phase,

$$\begin{aligned}
\beta\Delta\mu^{\mathrm{ex}}[n](\boldsymbol{r}) &\equiv \frac{\delta\beta\Delta\mathscr{F}^{\mathrm{ex}}[n; n_0]}{\delta n(\boldsymbol{r})} - \beta\mu^{\mathrm{ex}}(n_0) \qquad (19) \\
&= -\int \mathrm{d}\underline{\boldsymbol{r}} c^{(2)}(|\boldsymbol{r} - \underline{\boldsymbol{r}}|)\Delta n(\underline{\boldsymbol{r}}) \\
&\quad - \sum_{m=3}^{\infty} \frac{1}{m!} C^{(m)}(n_0)\left(\Delta n^{\mathrm{eff}}(\boldsymbol{r})\right)^{m-1} \\
&\quad - \sum_{m=3}^{\infty} \frac{m-1}{m!} C^{(m)}(n_0) \int \mathrm{d}\underline{\boldsymbol{r}} w(|\boldsymbol{r} - \underline{\boldsymbol{r}}|) \\
&\quad \times \left(\Delta n^{\mathrm{eff}}(\underline{\boldsymbol{r}})\right)^{m-2} \Delta n(\underline{\boldsymbol{r}}). \qquad (20)
\end{aligned}$$

Equations (17)–(20) are non-linear and can be solved iteratively.

To obtain the second-order DCF, we have to solve the Ornstein–Zernike equation,

$$\hat{h}(k) = \hat{c}^{(2)}(k) + n_0 \hat{h}(k)\hat{c}^{(2)}(k), \tag{21}$$

where h is the pair correlation function. From the Percus relation,[35] the pair correlation function is written as the conditional density distribution, given the external potential from the fixed identical particle,

$$h(r) = n_{\mathrm{eq}}[\mu(n_0) - u](r)/n_0 - 1, \tag{22}$$

where u is the pair potential between particles. Using this relation and Eqs. (17)–(21), we obtain the pair correlation function as

$$h(r) = \exp\left(-\beta u^{\mathrm{eff}}[h, c](r)\right) - 1, \tag{23}$$

$$\beta u^{\mathrm{eff}}[h, c](r) = \beta u(r) + c^{(2)}(r) - h(r) + b[h, c](r), \tag{24}$$

$$\begin{aligned}
b[h, c](|\boldsymbol{r}_1 - \boldsymbol{r}_2|) &= -\sum_{m=3}^{\infty} \frac{C^{(m)}(n_0)}{m!}\left(n_0 h^{\mathrm{eff}}(|\boldsymbol{r}_1 - \boldsymbol{r}_2|)\right)^{m-1} \\
&\quad - \sum_{m=3}^{\infty} \frac{m-1}{m!} C^{(m)}(n_0) \int \mathrm{d}\underline{\boldsymbol{r}} w(|\boldsymbol{r}_1 - \underline{\boldsymbol{r}}|) \\
&\quad \times \left(n_0 h^{\mathrm{eff}}(|\underline{\boldsymbol{r}} - \boldsymbol{r}_2|)\right)^{m-2} n_0 h(|\underline{\boldsymbol{r}} - \boldsymbol{r}_2|),
\end{aligned} \tag{25}$$

$$h^{\mathrm{eff}}(|\boldsymbol{r}_1 - \boldsymbol{r}_2|) \equiv \int \mathrm{d}\underline{\boldsymbol{r}} w(|\boldsymbol{r}_1 - \underline{\boldsymbol{r}}|)h(|\underline{\boldsymbol{r}} - \boldsymbol{r}_2|), \tag{26}$$

where u^{eff} is the effective pair potential and b is the bridge function. To enclose the equations, we need additional equations for higher-order DCFs. From Baxter's relation,[36] the higher-order DCFs at zero-wave vectors $\hat{\hat{c}}^{(m)}(k; n_0)$ are given as the density derivative of the second-order DCF,

$$\hat{\hat{c}}^{(m)}(k; n_0) \equiv \hat{c}^{(m)}(k, 0, \ldots, 0; n_0) = \frac{\partial^{m-2}}{\partial n_0^{m-2}}\hat{c}^{(2)}(k; n_0). \tag{27}$$

Using this relation, the density derivatives of Eqs. (21) and (23) give equations for higher-order DCFs,

$$\frac{\partial^i}{\partial n_0^i}\hat{h}(k) = \frac{\partial^i}{\partial n_0^i}\left(\hat{c}^{(2)}(k) + n_0\hat{h}(k)\hat{c}^{(2)}(k)\right), \tag{28}$$

$$\frac{\partial^i}{\partial n_0^i} h(r) = \frac{\partial^i}{\partial n_0^i} \exp\left(-\beta u^{\text{eff}}[h,c](r)\right). \tag{29}$$

Consequently, if we truncate the higher-order terms beyond the mth-order term, Eqs. (23)–(29) complete the self-consistent iteration to determine the second-order DCF, $c^{(2)}(r; n_0)$, and the Fourier transforms of DCFs at zero wave vector, $C^{(i)}(n_0)$ $(i = 3, \ldots, m)$. We hereinafter refer to these equations as hierarchal integral equations. The scheme for the solution of the equations is same as that described in our previous study.[34] First, we set the values of correlation functions as zero. Then, we start the calculation of the self-consistent loop for the pair correlation function, the DCF, and the effective potential. If the iteration is converged, next, we start the calculation of the self-consistent loop for the first derivatives. In the same way, we calculate the ith derivatives $(i = 1, \ldots, m)$ in order. After the calculation of the mth derivatives, we return to the first. This procedure is repeated until these become consistent with those obtained in the previous loop. Finally, the converged DCFs give the grand potential functional.

C. Truncation of long tail of weight function

In the long-range limit, the second-order DCFs behave asymptotically as $c^{(2)}(r) \to -\beta u(r)$ so that it cancels out the pair potential in the effective pair potential.[3] This long range behavior of DCFs represents the shielding effect to the long tail of the pair potential. The weight function that is defined as the normalized second-order DCF also has the same long-range behavior. The long tail of the weight function causes the unphysical slow decay of the bridge function. This behavior violates the shielding of pair potential and makes the solution of the hierarchical integral equations diverge. From the asymptotic form of $c^{(2)}(r)$, we can presume that the density dependence of the long-range part of the second-order DCF is relatively weak compared with the core part. Because the bridge functional consists of density derivatives of the second-order DCF, we should neglect the long-range part of the weight function for constructing the bridge functional. To account for the short-range nature of the bridge functional, we truncate the long tail of the weight function and redefine the weight function in the core region. Following the Weeks–Chandler–Andersen (WCA) theory,[38] we truncate the DCF at the location of the minimum point of the pair potential, $r_{\min}$, and define the weight function as

$$w_{\text{tr}}(r) = \frac{t(|\boldsymbol{r}_1 - \boldsymbol{r}_2|)}{\hat{t}(0)}, \tag{30}$$

$$t(r) = \begin{cases} c^{(2)}(r) & (r < r_{\min}), \\ 0 & (r \geq r_{\min}). \end{cases} \tag{31}$$

We can use other truncation protocols for determination of the cut-off distance such as the Barker–Henderson (BH) theory.[37] We have numerically compared the solutions of the hierarchical integral equations obtained from the WCA and the BH protocol to check the sensitivity to the cut-off distance and confirmed that the two results were almost indistinguishable from each other. In the following calculation, we use the truncated weight function with the WCA protocol instead of Eq. (15).

III. APPLICATION TO LENNARD-JONES FLUID

A. Computational details

We applied the new method to Lennard-Jones (LJ) fluids whose particles interact via the pair potential,

$$u_{\text{LJ}}(r) = 4\varepsilon_{\text{v}}\left[\left(\frac{\sigma_{\text{v}}}{r}\right)^{12} - \left(\frac{\sigma_{\text{v}}}{r}\right)^{6}\right], \tag{32}$$

where ε_{v} and σ_{v} are the depth of the potential well and the diameter of the particle, respectively. The reduced temperature is $T^* = k_B T/\varepsilon_{\text{v}}$, and the reduced density is $n^* = n\sigma_{\text{v}}^3$. We fix the density at $n_0^* = 0.70$, which corresponds to a liquid state, and focus on the four temperatures $T^* = 0.90, 1.00, 1.20$, and 2.40. These states correspond to the meta-stable state, the liquid–vapor equilibrium state, subcritical state, and supercritical state, respectively.

The hierarchical integral equations [Eqs. (23)–(29)] truncated to the fourth-order were solved using the fast Fourier transform. The number of grid points was set as 10 000 to obtain the smooth solutions. The maximum value of the radial distance was set to $30.0\sigma_{\text{v}}$. The obtained DCFs were used for the grand potential functional in the inhomogeneous system calculation. The self-consistent equations for the inhomogeneous fluids [Eqs. (17)–(20)] were solved using the fast Fourier transform with 10 000 linear grids. The method of modified direct inversion in the iterative subspace (MDIIS)[39] was employed to solve the equations for both the homogeneous and inhomogeneous fluids. It ensured great acceleration and stability of convergence.

B. Grand potential density for uniform system

We define the grand potential density relative to equilibrium uniform state as a function of uniform density n,

$$\beta\Delta\omega(n;\mu(n_0)) \equiv \beta\Delta\Omega(n;\mu(n_0))/V, \tag{33}$$

$$= n\ln\frac{n}{n_0} - \Delta n - \sum_{m=2}^{\infty}\frac{C^{(m)}(n_0)}{m!}(\Delta n)^m, \tag{34}$$

where $\Delta n = n - n_0$. If the uniform phase at density n is equilibrium with that at density n_0, the grand potential density satisfies

$$\Delta\omega(n;\mu(n_0)) = \frac{\partial}{\partial n}\Delta\omega(n;\mu(n_0)) = 0. \tag{35}$$

In Fig. 1, we estimated the value of $\Delta\omega(n;\ \mu(n_0))$ from the modified Benedict–Webb–Rubin equation of state (EOS), which gives the polynomial function for the Helmholtz free energy density of the LJ fluid.[40] This equation accurately predicts the liquid–vapor coexisting curve. At the supercritical condition, $T^* = 2.4$, the curve of the grand potential is almost parabolic. As the temperature decreases, the grand potential decreases in the low-density region that corresponds to the vapor state. At the liquid–vapor equilibrium condition, $T^* = 1.0$, the grand potential curve shows the local minimum at $n^* = 0.028$. At this point, the value of the grand potential is equivalent to that at the reference density $n^* = n_0^* = 0.7$ and the phase equilibrium condition is satisfied. The further decrease in the temperature lowers the grand potential at the low-density region and reverses the relative stability between the liquid and vapor phase.

We show the result from the fourth-order expansion obtained from the hierarchical integral equations. For all the conditions,

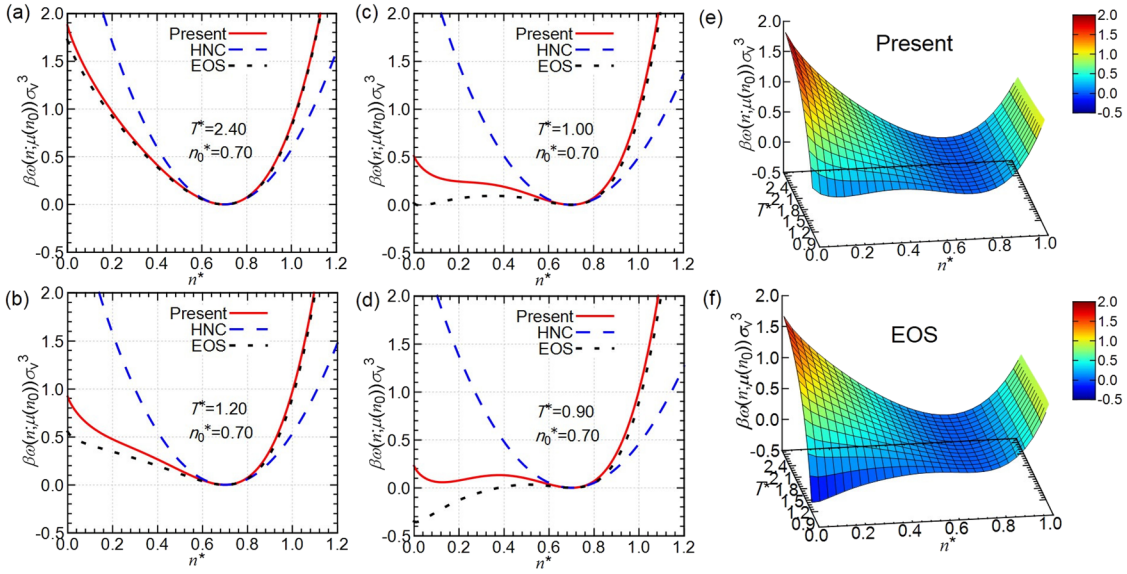

FIG. 1. The grand potential density of the uniform system as a function of reduced density n^* for (a) $T^* = 2.40$, (b) 1.20, (c) 1.00, and (d) 0.90. We also present the two dimensional plots of the grand potential density as a function of n^* and T^*, which is obtained from (e) the present functional and (f) the modified Benedict–Webb–Rubin equation of state. In each plot, we set the chemical potential as $\mu(n_0^* = 0.70)$.

the truncation beyond the second-order term corresponding to the HNC approximation gives the almost quadratic function centered at $n^* = n_0^*$. The HNC largely overestimated the value in the low-density region. Conversely, the value in the high-density region is underestimated. On the other hand, the prediction of the present functional, which includes third- and fourth-order terms, gives good agreement with the EOS results, except in the low-density and low-temperature regions. The 3D-plots clearly display this feature. Owing to the overestimation in the low-density and low-temperature regions, the present functional fails to predict the liquid–vapor equilibrium at $T^* = 1.0$. At the lower temperature $T^* = 0.9$, it gives the two local minima that are very close to the liquid–vapor equilibrium. Although the present functional underestimates the equilibrium temperature, it qualitatively predicts the liquid–vapor equilibrium.

C. Solvation around hard sphere solute

We discuss the solvation around a hard-sphere (HS) with varying sizes. The external potential produced by the HS solute is

$$v(r) = \begin{cases} \infty & r \le D, \\ 0 & r > D, \end{cases} \tag{36}$$

where D is the diameter of the spherical cavity that is produced by the hard-core potential. The reduced diameter is defined as $D^* = D/\sigma_v$.

In Fig. 2(a), we plot the contact values of the reduced density distribution, $n(D)/n_0$. The contact values provide a systematic check of the drying behavior near the solute surface. The values calculated by the HNC approximation are insensitive to the temperature and almost reach large plateau values at $D^* = 2.0$. On the other hand, for the results from the present functional, the contact values decrease as the temperature decreases and the diameter increases. Clearly, the features of drying are predicted by the present functional.

The solvation free energy (SFE) is given by the grand potential relative to the equilibrium homogeneous state at equilibrium density,

$$\Delta^{\rm solv}\Omega \equiv \Delta\Omega[n_{\rm eq}; \mu(n_0) - v], \tag{37}$$

$$= -k_B T \int d\boldsymbol{r} \Delta n(\boldsymbol{r}) - \int d\boldsymbol{r} n(\boldsymbol{r}) \Delta\mu^{\rm ex}(\boldsymbol{r}) - \frac{1}{2}\int d\boldsymbol{r}_1 \int d\boldsymbol{r}_2 c^{(2)}(|\boldsymbol{r}_1 - \boldsymbol{r}_2|)\Delta n(\boldsymbol{r}_1)\Delta n(\boldsymbol{r}_2) - \sum_{m=3}^{\infty} \frac{1}{m!} C^{(m)}(n_0) \int d\boldsymbol{r}_1 \left(\Delta n^{\rm eff}(\boldsymbol{r}_1)\right)^{m-1} \Delta n(\boldsymbol{r}_1). \tag{38}$$

In Fig. 2(b), we plot the solute size dependence of the SFE per surface area of the cavity, which is scaled by the inverse temperature, $\beta\Delta^{\rm solv}\Omega/\pi D^{*2}$. Similar to the contact values, the SFE calculated by the HNC approximation is insensitive to the temperature. For the present functional, the decrease in the temperature lowers the slope of the SFE curve. For $T^* = 0.90$, the SFE is very close to the plateau curve.

For the comparison with Monte Carlo (MC) simulation results by Ashbaugh (MC-A)[42] and Huang and Chandler (MC-HC),[41] we performed calculations for the LJ fluids with the potential truncated and shifted at $2.5\sigma_v$,

$$\tilde{u}_{\rm LJ}(r) = \begin{cases} u_{\rm LJ}(r) - u_{\rm LJ}(2.5\sigma_v) & (r \le 2.5\sigma_v), \\ 0 & (r > 2.5\sigma_v). \end{cases} \tag{39}$$

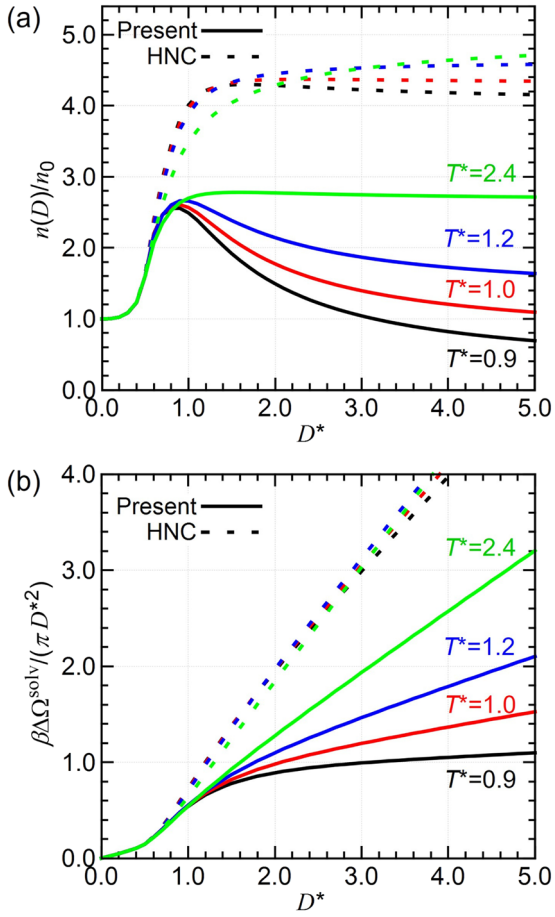

FIG. 2. (a) The contact value of reduced density and (b) the solvation free energy of Lennard-Jones fluids around a hard sphere (HS) as a function of HS diameter D^*.

The thermodynamic conditions are set as $T^* = 0.85$ and $n_0^* = 0.70$, which is close to the liquid–vapor coexistence. In Fig. 3(a), we plot the grand potential for the uniform system. The grand potential curve obtained from the EOS shows the local minimum at $n^* = 0.02$. As in the case of the normal LJ system, the present functional slightly overestimates the grand potential in the low-density region and misses the quantitative prediction of the liquid–vapor equilibrium.

In Fig. 3(b), we plot the contact value of the reduced density distribution $n(D)/n_0$. The MC results show the maximum around $D^* = 1.0$ and then decrease with the solute diameter D. For the small size of the solute, $D^* = 0.5$, the results of the HNC and present functional are almost indistinguishable from each other and agree well with simulation data. The present functional qualitatively reproduces the feature of the depletion for the large D limit. In the HNC results, large positive deviations from the simulation data are observed for $D^* > 0.5$ and these values are greatly larger than unity.

Figure 3(c) shows the cavity solvation free energy predicted by DFT and MC simulations. The SFE of the MC result reaches a plateau for large D values, giving a value for surface free energy γ. In the macroscopic limit, the SFE is written as the sum of the volumetric term and the surface term, $\Delta^{\mathrm{solv}}\Omega = P\pi D^3/6 + \gamma\pi D^2$. The volumetric term is represented by the grand potential for uniform systems, $\Delta\omega(0;\ \mu(n_0))\pi D^3/6$. As shown in Fig. 3(a), this term is negligible at the condition close to the liquid–vapor equilibrium. The present functional largely improves the agreement with the MC result. However, the overestimation of the grand potential for uniform systems in the low-density region results in the finite slope of the SFE at large D. For the previous DFT study, the HSRF method by Wu,[43] the SFE values also do not reach a plateau in the limit of large D.

D. Solvation around Lennard-Jones solute

We also apply the obtained functional to the solvation around the LJ solute. The external potential is given by

$$v(r) = 4\sqrt{\varepsilon_{\mathrm{v}}\varepsilon_{\mathrm{u}}}\left[\left(\frac{\sigma_{\mathrm{v}}+\sigma_{\mathrm{u}}}{2r}\right)^{12} - \left(\frac{\sigma_{\mathrm{v}}+\sigma_{\mathrm{u}}}{2r}\right)^{6}\right], \tag{40}$$

where ε_{u} and σ_{u} are the LJ parameters for the solute. The well-depth parameter ε_{u} is taken identical to ε_{v}. The reduced diameter is defined as $\sigma_{\mathrm{u}}^* = \sigma_{\mathrm{u}}/\sigma_{\mathrm{u}}$

We calculated the radial distribution function $g(r)$ of LJ fluids ($n_0^* = 0.70$ and $T^* = 1.20$) around the LJ solute ($\sigma_{\mathrm{u}}^* = 1.0$ and 3.0). In Fig. 4, we show $g(r)$ obtained from the DFT methods and molecular dynamics (MD) simulation result by Miyata and Thapa,[44] focusing on the first peak. For the HNC approximation, we observe a shift of

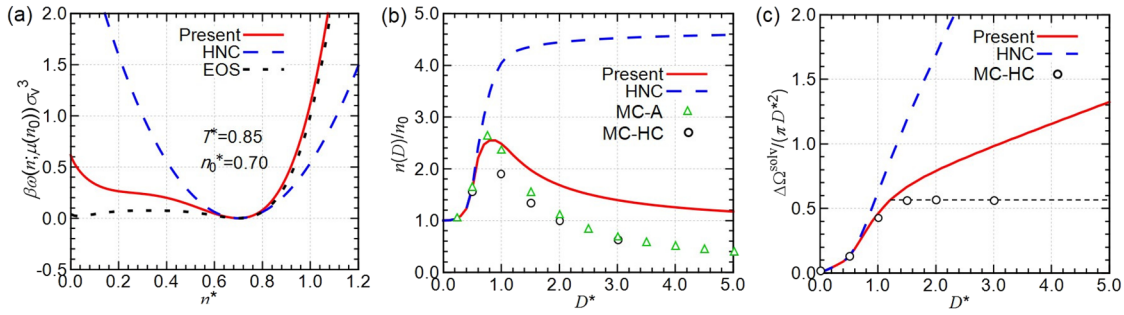

FIG. 3. The comparison with the equation of state and Monte Carlo simulation data. (a) The grand potential density for the homogeneous system. (b) The contact value of the reduced density. (c) The solvation free energy. The black dashed line shows a plateau suggested by MC.

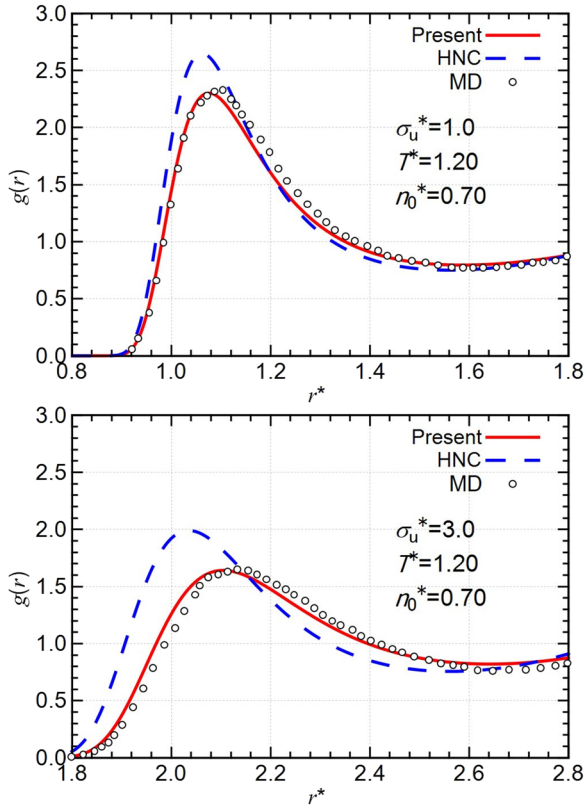

FIG. 4. Comparison of the radial distribution functions for the LJ fluids around the LJ solute.

the first peak position toward a shorter distance than the MD result. The shift in the result for $\sigma_u^* = 3.0$ is larger than that for $\sigma_u = 1.0$. The present method shows good agreement in the position and the height of the first peak. However, the shoulder of the first peak is slightly deviated from the MD result. The similar deviation in the shoulder was observed in the HSRF method.[9]

Figure 5 shows the solute size dependence of the SFE for the LJ solute at $T^* = 0.9, 1.0, 1.2$, and 2.4. To compare with the simulation data, we plot the molecular dynamics (MD) simulation result of Miyata *et al.*[44,45] at $T^* = 1.2$ and 2.4. The SFE value when σ_u is identical to σ_v corresponds to the excess chemical potential for the pure LJ fluid. In this case, the HNC gives a SFE value relatively close to that obtained from the MD simulation. As the size of the solute increases, the SFE value calculated by the MD simulation monotonically increases for $T^* = 2.4$ and decreases for $T^* = 1.2$. In contrast to the results obtained by the MD simulation, for both the conditions, the SFE value determined by HNC increases as the size of the solute increases. As a result, HNC produces a large value of the SFE for large solutes. As in the case of solvation around the HS solute, the overestimation of the volumetric term leads to a large value of the SFE. On the other hand, the present functional greatly improves the overestimation of the SFE, thus yielding good agreement with the results obtained by the MD simulation.

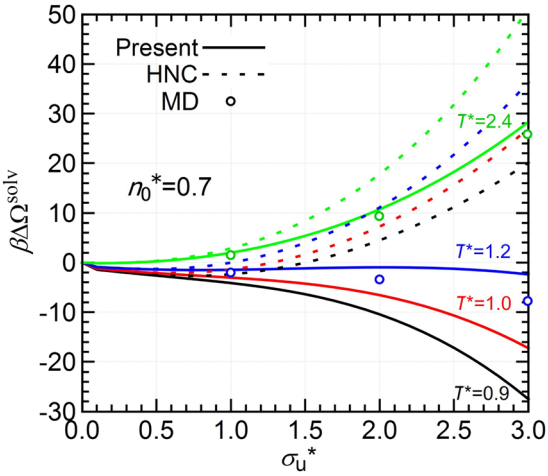

FIG. 5. The solvation free energy of Lennard-Jones fluids around a Lennard-Jones solute as a function of diameter σ_u^*.

IV. CONCLUSION

This paper presented the method for self-consistently constructing the grand potential density functional utilizing the hierarchical integral equations. We started by deriving the density expansion of the excess free energy functional. The central tool in this derivation is a weighted density approximation. The expansion coefficients are given in the Ornstein–Zernike integral equations with Baxter's relation. Using the test particle scheme of Percus, we provided the hierarchical integral equations for self-consistently constructing the grand potential functional.

The present functional was tested by application to the solvation thermodynamics of Lennard-Jones fluids. Compared to the modified Benedict–Webb–Rubin equation of state, the present functional qualitatively predicts the liquid–vapor equilibrium. The solvation free energy obtained from the present functional provides a much better agreement with the Monte Carlo simulation results than the HNC functional. The present method constitutes a general starting point for a systematic improvement in the accuracy of the grand potential functional and makes it possible to study a wide variety of physical phenomena.

ACKNOWLEDGMENTS

This work was supported by the JSPS KAKENHI (Grant Nos. JP17H03009 and JP20J15602). The management of Elements Strategy Initiative for Catalysts and Batteries (ESICB) is also acknowledged. Theoretical computations were partly performed at the Research Center for Computational Science, Okazaki, Japan.

AUTHOR DECLARATIONS

Conflict of Interest

The authors have no conflicts to disclose.

DATA AVAILABILITY

The data that support the findings of this study are available from the corresponding author upon reasonable request.

REFERENCES

[1] R. Evans, "The nature of the liquid-vapour interface and other topics in the statistical mechanics of non-uniform, classical fluids," Adv. Phys. **28**, 143 (1979).
[2] *Fundamentals of Inhomogeneous Fluids*, edited by J. R. Henderson (Marcel Dekker, New York, 1992).
[3] J.-P. Hansen and I. R. McDonald, *Theory of Simple Liquids*, 3rd ed. (Academic, London, 2006).
[4] R. Evans, P. Tarazona, and U. M. B. Marconi, "On the failure of certain integral equation theories to account for complete wetting at solid-fluid interfaces," Mol. Phys. **50**, 993 (1983).
[5] M. Oettel, "Integral equations for simple fluids in a general reference functional approach," J. Phys.: Condens. Matter **17**, 429 (2005).
[6] A. Ayadim, M. Oettel, and S. Amokrane, "Optimum free energy in the reference functional approach for the integral equations theory," J. Phys.: Condens. Matter **21**, 115103 (2009).
[7] M. Levesque, R. Vuilleumier, and D. Borgis, "Scalar fundamental measure theory for hard spheres in three dimensions: Application to hydrophobic solvation," J. Chem. Phys. **137**, 034115 (2012).
[8] G. Jeanmairet, M. Levesque, V. Sergiievskyi, and D. Borgis, "Molecular density functional theory for water with liquid-gas coexistence and correct pressure," J. Chem. Phys. **142**, 154112 (2015).
[9] T. Sumi, Y. Maruyama, A. Mitsutake, and K. Koga, "A reference-modified density functional theory: An application to solvation free-energy calculations for a Lennard-Jones solution," J. Chem. Phys. **144**, 224104 (2016).
[10] D. Borgis, S. Luukkonen, L. Belloni, and G. Jeanmairet, "Simple parameter-free bridge functionals for molecular density functional theory. Application to hydrophobic solvation," J. Phys. Chem. B **124**, 6885–6893 (2020).
[11] D. Borgis, S. Luukkonen, L. Belloni, and G. Jeanmairet, "Accurate prediction of hydration free energies and solvation structures using molecular density functional theory with a simple bridge functional," J. Phys. Chem. **155**, 024117 (2021).
[12] P. Tarazona, "Free-energy density functional for hard spheres," Phys. Rev. A **31**, 2672 (1985).
[13] W. A. Curtin and N. W. Ashcroft, "Weighted-density-functional theory of inhomogeneous liquids and the freezing transition," Phys. Rev. A **32**, 2909 (1985).
[14] D. M. Kroll and B. B. Laird, "Comparison of weighted-density-functional theories for inhomogeneous liquids," Phys. Rev. A **42**, 4806 (1990).
[15] A. R. Denton and N. W. Ashcroft, "Weighted-density-functional theory of nonuniform fluid mixtures: Application to the structure of binary hard-sphere mixtures near a hard wall," Phys. Rev. A **44**, 8242 (1991).
[16] C. N. Patra and S. K. Ghosh, "A simple weighted-density-functional approach to the structure of inhomogeneous fluids," J. Chem. Phys. **116**, 8509 (2002).
[17] C. N. Patra and S. K. Ghosh, "A self-consistent weighted-density-functional approach to the structure of simple fluids," J. Chem. Phys. **116**, 9845 (2002).
[18] C. N. Patra and S. K. Ghosh, "Structure of nonuniform three-component fluid mixtures: A density-functional approach," J. Chem. Phys. **118**, 8326 (2003).
[19] T. Sumi and H. Sekino, "A self-consistent density-functional approach for homogeneous and inhomogeneous classical fluids," J. Phys. Soc. Jpn. **77**, 034605 (2008).
[20] A. R. Denton and N. W. Ashcroft, "Modified weighted-density-functional theory of nonuniform classical liquids," Phys. Rev. A **39**, 4701 (1989).
[21] J. F. Lutsko and M. Baus, "Nonperturbative density-functional theories of classical nonuniform systems," Phys. Rev. A **41**, 6647 (1990).
[22] C. N. Likos and N. W. Ashcroft, "Self-consistent theory of freezing of the classical one-component plasma," Phys. Rev. Lett. **69**, 316 (1992).
[23] R. Leidl and H. Wagner, "Hybrid WDA: A weighted-density approximation for inhomogeneous fluids," J. Chem. Phys. **98**, 4142 (1993).
[24] S. C. Kim and S. H. Suh, "Weighted-density approximation and its application to classical fluids," J. Chem. Phys. **104**, 7233 (1996).
[25] Y. Rosenfeld, "Free-energy model for the inhomogeneous hard-sphere fluid mixture and density-functional theory of freezing," Phys. Rev. Lett. **63**, 980 (1989).
[26] E. Kierlik and M. L. Rosinberg, "Free-energy density functional for the inhomogeneous hard-sphere fluid: Application to interfacial adsorption," Phys. Rev. A **42**, 3382 (1990).
[27] P. Tarazona, "Density functional for hard sphere crystals: A fundamental measure approach," Phys. Rev. Lett. **84**, 694 (2000).
[28] R. Roth, R. Evans, A. Lang, and G. Kahl, "Fundamental measure theory for hard-sphere mixtures revisited: The white bear version," J. Phys.: Condens. Matter **14**, 12063 (2002).
[29] Y.-X. Yu and J. Wu, "Structures of hard-sphere fluids from a modified fundamental-measure theory," J. Chem. Phys. **117**, 10156 (2002).
[30] H. Hansen-Goos and R. Roth, "A new generalization of the Carnahan-Starling equation of state to additive mixtures of hard spheres," J. Phys.: Condens. Matter **18**, 8413 (2006).
[31] H. Hansen-Goos and K. Mecke, "Fundamental measure theory for inhomogeneous fluids of nonspherical hard particles," Phys. Rev. Lett. **102**, 018302 (2009).
[32] R. Roth, "Fundamental measure theory for hard-sphere mixtures: A review," J. Phys.: Condens. Matter **22**, 063102 (2010).
[33] J. F. Lutsko, "Explicitly stable fundamental-measure-theory models for classical density functional theory," Phys. Rev. E **102**, 062137 (2020).
[34] T. Yagi and H. Sato, "Self-consistent construction of bridge functional based on the weighted density approximation," J. Chem. Phys. **154**, 124113 (2021).
[35] J. K. Percus, "Approximation methods in classical statistical mechanics," Phys. Rev. Lett. **8**, 462 (1962).
[36] R. J. Baxter, "Direct correlation functions and their derivatives with respect to particle density," J. Chem. Phys. **41**, 553 (1964).
[37] J. A. Barker and D. Henderson, "Perturbation theory and equation of state for fluids. II. A successful theory of liquids," J. Chem. Phys. **47**, 4714 (1967).
[38] J. D. Weeks, D. Chandler, and H. C. Andersen, "Role of repulsive forces in determining the equilibrium structure of simple liquids," J. Chem. Phys. **54**, 5237 (1971).
[39] A. Kovalenko, S. Ten-no, and F. Hirata, "Solution of the three-dimensional RISM/HNC equations for SPC water by the modified method of direct inversion in the iterative subspace," J. Comput. Chem. **20**, 928 (1999).
[40] J. K. Johnson, J. A. Zollweg, and K. E. Gubbins, "The Lennard-Jones equation of state revisited," Mol. Phys. **78**, 591–618 (1993).
[41] D. M. Huang and D. Chandler, "Cavity formation and the drying transition in the Lennard-Jones fluid," Phys. Rev. E **61**, 1501 (2000).
[42] H. S. Ashbaugh, "Blowing bubbles in Lennard-Jonesium along the saturation curve," J. Chem. Phys. **130**, 204517 (2009).
[43] J. Wu, "Solvation of a spherical cavity in simple liquids: Interpolating between the limits," J. Phys. Chem. B **113**, 6813–6818 (2009).
[44] T. Miyata and J. Thapa, "Accuracy of solvation free energy calculated by hypernetted chain and Kovalenko–Hirata approximations for two-component system of Lennard-Jones liquid," Chem. Phys. Lett. **604**, 122 (2014).
[45] T. Miyata and Y. Ebato, "Correction of Kovalenko-Hirata closure in Ornstein-Zernike integral equation theory for Lennard-Jones fluids," J. Mol. Liq. **245**, 2–10 (2017).